Collateral damage: Evolution with displacement of fracture distribution and secondary fault strands in fault damage zones

Heather M. Savage[1,2] and Emily E. Brodsky[1]

Received 22 April 2010; revised 10 December 2010; accepted 28 December 2010; published 31 March 2011.

[1] We investigate the development of fracture distributions as a function of displacement to determine whether damage around small and large faults is governed by the same process. Based on our own field work combined with data from the literature, we find that (1) isolated single faults with small displacements have macrofracture densities that decay as $r^{-0.8}$, where r is distance from the fault plane, (2) mature fault damage zones can be interpreted as a superposition of these $r^{-0.8}$ decays from secondary fault strands, resulting in an apparently more gradual decay with distance, and (3) a change in apparent decay and fault zone thickness becomes evident in faults that have displaced more than ~150 m. This last observation is consistent with a stochastic model where strand formation is related to the number of fractures within the damage zone, which in turn is a function of displacement. These three observations together suggest that the apparent break in scaling between small and large faults is due to the nucleation of secondary faults and not a change in process.

Citation: Savage, H. M., and E. E. Brodsky (2011), Collateral damage: Evolution with displacement of fracture distribution and secondary fault strands in fault damage zones, *J. Geophys. Res.*, *116*, B03405, doi:10.1029/2010JB007665.

1. Introduction

[2] Most fault cores are enveloped by a halo of pervasive cracking known as the damage zone, which decays in intensity away from the fault [e.g., *Brock and Engelder*, 1977; *Chester and Logan*, 1986]. An important question in fault and earthquake mechanics is how these damage zones form and whether the same mechanisms govern damage zone development throughout the growth of the fault. Fracturing mechanisms could include the quasi-static stress field, dynamic shaking, the process zone associated with the rupture tip, fault geometry, and linkage [e.g., *Rispoli*, 1981; *Vermilye and Scholz*, 1998; *Rice et al.*, 2005; *Childs et al.*, 2009]. One way that this question has been approached is through the study of how fault damage zones scale with displacement [e.g., *Beach et al.*, 1999; *Fossen and Hesthammer*, 2000; *Shipton et al.*, 2006; *Childs et al.*, 2009; *Mitchell and Faulkner*, 2009]. A break in the scaling of fault zones could suggest that the processes involved in creating damage change as the fault core matures. However, damage zones around larger faults may be more difficult to interpret than small faults due to overprinting from multiple slip events.

[3] Previous studies of damage zone scaling have focused on the fault length to thickness ratio [e.g., *Vermilye and Scholz*, 1998], along-strike variations in damage [e.g., *Shipton et al.*, 2005], types of damage measured [*Schulz and Evans*, 2000] and/or the scaling of damage zone thickness with displacement [e.g., *Knott et al.*, 1996; *Beach et al.*, 1999]. Here we focus on the decay of damage away from the fault as a function of displacement as well as the scaling of damage thickness with displacement. Previous studies have shown that damage (i.e., macroscopic fractures, microfractures, deformation bands) decays sharply with distance from the fault core [*Brock and Engelder*, 1977; *Chernyshev and Dearman*, 1991; *Anders and Wiltschko*, 1994; *Vermilye and Scholz*, 1998; *Chester et al.*, 2005; *Mitchell and Faulkner*, 2009]. Here we use this decay, or spatial gradient, of density as a diagnostic of fault evolution. Because the decay directly captures the variation in fracture density with distance from the fault surface, it is unambiguously related to the faulting process.

[4] In this paper, we systematically build an understanding of the damage falloff around faults with varying maturity by beginning with measurements of the distribution and extent of damage around small faults with minimal overprinting. We focus particularly on the falloff of damage as a function of distance from the fault as the gradient of damage is less dependent on the local lithology than the absolute number of fractures. Next we combine these new data with published data on larger faults of all rock types to establish the scaling of fault damage with displacement. We show that damage zone thickness and falloff is a function of total

[1]Department of Earth and Planetary Sciences, University of California, Santa Cruz, California, USA.
[2]Now at Lamont-Doherty Earth Observatory, Columbia University, Palisades, New York, USA.

0148-0227/11/2010JB007665

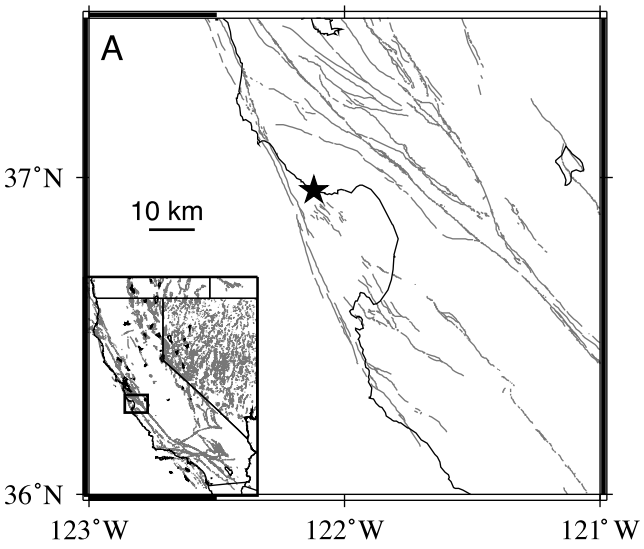

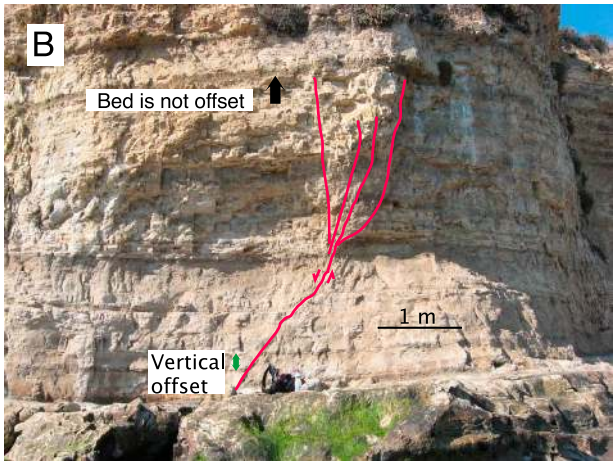

Figure 1. (a) Location of Four Mile Beach (black star). Black lines are California coast. (b) Low Tide Fault at Four Mile Beach. The fault (red) ends near the top of the cliff, where it splays.

fault displacement. Finally, we attribute an observed change of damage scaling to the formation of secondary fault strands and model the damage distribution around large faults as overlapping damage zones of multiple, secondary fault strands, using the same damage distribution found for the smallest faults. By superposing the damage distribution found around small faults onto secondary strands, we successfully recreate the more complex damage distributions found around large faults, without invoking a change in physics of fault zones with increasing maturity.

2. Small Faults: Four Mile Beach, California

[5] We analyze damage around faults by examining faults with relatively small offsets and well-developed damage zones. For this part of the study, we measure the decay of damage around three small, isolated, normal faults located west of Santa Cruz, California (Figure 1). Fracture density decay robustly captures features associated with faulting by focusing on the systematic variations with distance from the fault. Because the falloff of microfracture and macrofracture density can differ for the same fault [*Schulz and Evans*, 1998], here we only consider macroscale features.

2.1. Description of Host Rock and Faults

[6] The host rock at Four Mile Beach is Santa Cruz Mudstone. This rock is a late Miocene age medium to thickly bedded (~10 cm near the faults in this study), organic siliceous mudstone [*Clark*, 1981]. There are interbeds of organic-rich mudstones that are darkly colored and more brittle than the thicker mudstone beds with which they alternate. The degree of coupling varies between the layers. At Low Tide Fault (Figure 1b), some of the layers are mechanically well coupled, as evidenced by fractures continuing across layer boundaries. At Hackle Fault, fractures in the darker layers tend to be vertical whereas the fractures in the lighter mudstone tend to be at an angle to the principal stress direction, assuming Andersonian faulting. We interpret this to be because the thinner, more brittle dark mudstone fractured before the lighter mudstone layers. At Three Mile Fault there is only one organic-rich layer, as well as some more thinly laminated light colored mudstone layers. Fractures mostly continue across layer boundaries at this fault. The vertical offset of beds is 0.35–0.7 m on the faults.

2.2. Background Fracture Density

[7] The background fracture density varied between ~9–15 fractures/meter in the layers around the faults. The difference in background density is related to the fracture resistance of the layer. The background fractures surrounding Low Tide Fault are generally vertical and fracture orientation rotates with proximity to the fault (Figure 2). Hackle and Three Mile faults have vertical fractures as well as dipping conjugate shear fractures. In order to account for the differences in fracture resistance, we subtract the background density from each layer. This result is the same (within error) as fitting each individual transect and taking the mean of the fits; however, this method is more robust because it minimizes heterogeneities in any one transect. Although shear fractures are present in the damage zone, there are no well-developed secondary fault strands with more than a few centimeters of displacement and its own fault core.

2.3. Fracture Density From Transects at Four Mile Beach

[8] On each fault, we measured several horizontal linear transects using a measuring tape to mark the distance of each fracture from the fault, taking care to remain within a single bed for each transect. We then make a geometric correction with fault dip to determine the perpendicular distance from the fault, as well as a geometric correction for the strike of the cliff face. We take multiple transects at each site in order to diminish the effects of noncontinuous features and local heterogeneity. Linear transects were preferred over other methods like line length over area methods to avoid smoothing problems related to discontinuous sampling (discussed further in section 3). Both shear fractures and joints were counted. Transect lengths were generally one

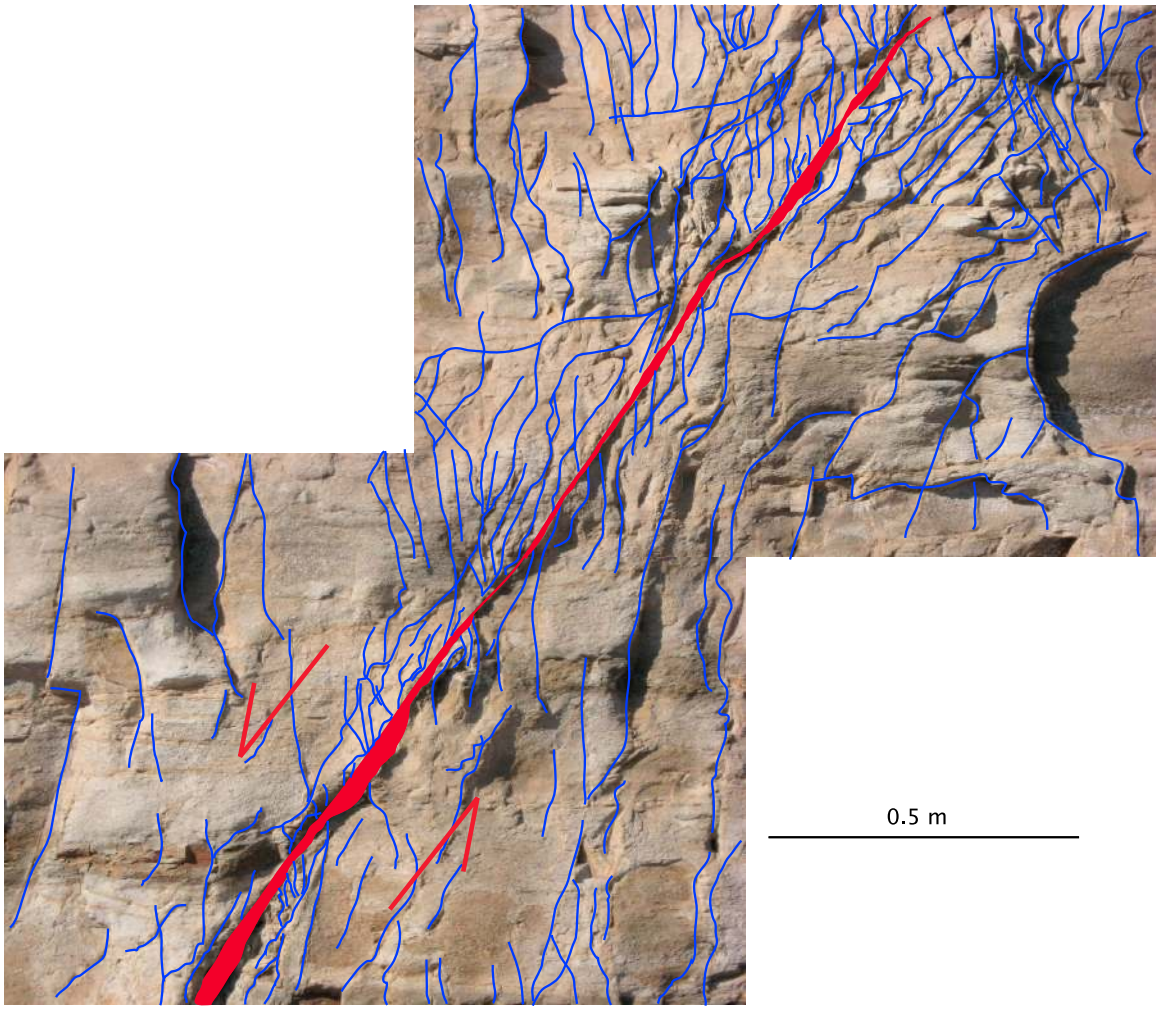

Figure 2. Low Tide Fault. The fault core is red, and the fractures surrounding the fault are blue. Fractures are nearly vertical away from the fault and rotate with proximity to the fault.

meter in perpendicular distance from the fault and the damage zone thickness was determined by the point where fracture density fell to background levels (in all cases the thickness was much smaller than the length of the transects).

[9] We measured the decay in fracture density between the fault core and the edge of the damage zone and found a strong decay well fit by a power law function:

$$d = cr^{-n} \tag{1}$$

where d is fracture density in units of number per meter, r is distance from the fault, n is an exponent describing the decay, and c is a constant that is fault-specific. As is appropriate for power law fits, we present the data in Figure 3 on a log-log plot where the slope of a linear regression is n [*Steele and Torrie*, 1980]. Other possible functions that fit the data are described in section 3. The value of n for the three small faults ranges from 0.67 ± 0.11 to 0.82 ± 0.14. Errors are the mean absolute deviation from 10,000 bootstrap resamplings of each fracture data set. Based on this first example, we provisionally conclude that small, isolated faults have a well-defined average density decay that is relatively steep ($n \approx 0.8$).

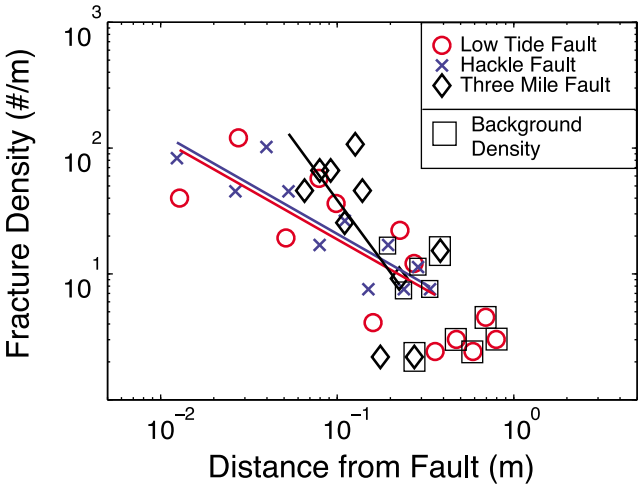

Figure 3. Representative transects of fracture density with distance from the fault core for small faults. The boxes represent the background fracture density. A total of nine, five, and five transects were collected on both sides of each fault for Low Tide, Hackle, and Three Mile faults, respectively.

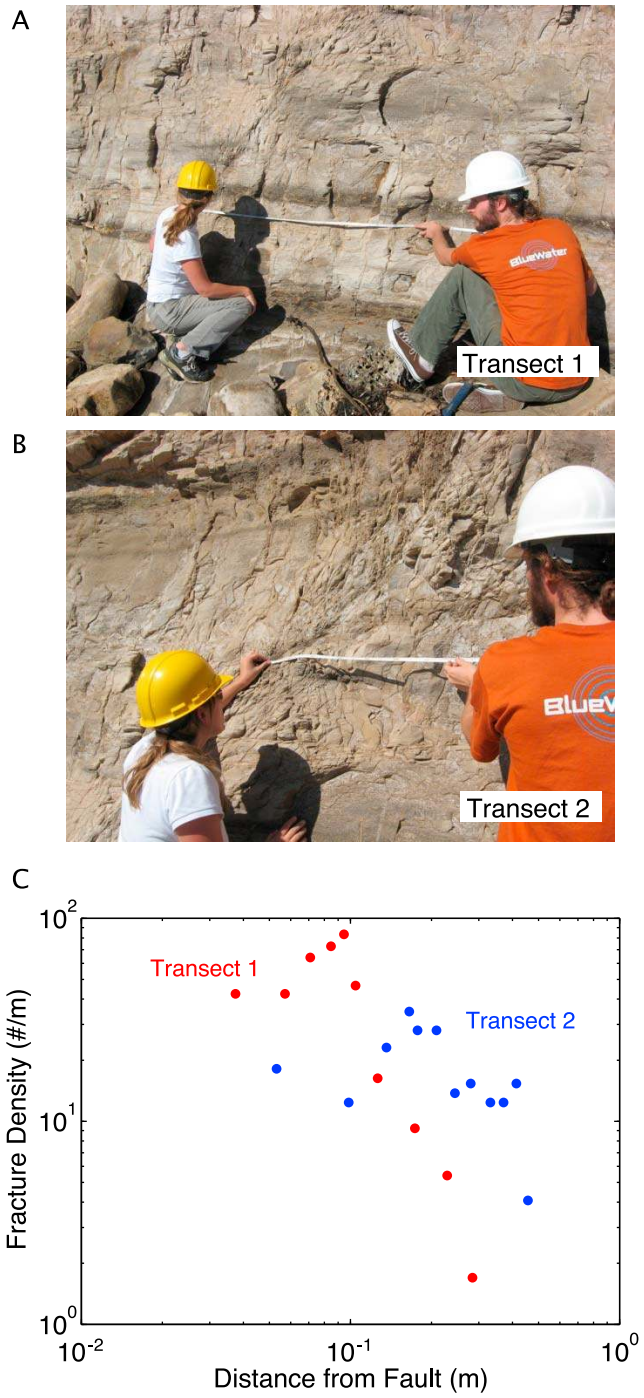

Figure 4. (a) Photo of transect 1, taken in straighter section of fault below transect 2. (b) Photo of transect 2 taken near bend in Low Tide Fault. (c) Change in fracture density decay associated with the bend in the fault.

[10] When comparing individual transects, the most distinct change in fracture falloff occurs where transects are taken near more complicated fault geometry. For instance, the fracture density falloff around Low Tide Fault is based on nine transects, taken in different lithologic layers and on both sides of the fault. The section of the fault ranging from its intersection with the wave-cut platform up to ~2 m above the platform is fairly straight, and the fracture falloff looks similar in the transects taken in this region. However, when the fault bends, there is a clear change in the falloff of fracture density (Figure 4). The transect taken near the fault bend (transect 2) show an increase in damage zone thickness and a decrease in the decay exponent. If only areas around the fault bend were measured, the density decay would be shallower. Additionally, just above the area on the fault where transects were taken, the fault branches into several strands and ends (Figure 1). If transects were taken at this fault tip, the falloff of fracture density would be very gradual. We measured transects at several different locations along the fault and our measurement is an average for the whole fault.

3. Fracture Density Decay as a Function of Displacement

[11] To investigate the evolution of damage distribution with displacement, we combined our own results with published fracture density profiles (Figure 5 and Table 1). We report the displacement along the fault as reported by the authors, which in most cases is vertical or horizontal

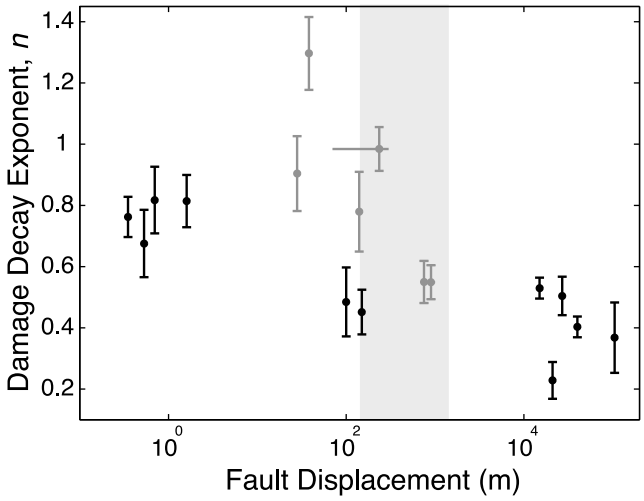

Figure 5. Damage decay exponent of the power law fit as a function of fault displacement. Error bars represent the mean absolute deviation from bootstrapping on 10,000 realizations. The points shown in gray represent data sets that have been binned; actual decay may be less steep than reported here. For instance, the points from the study at Four Mile Beach would have decay exponents closer to one if data were binned. The gray zone represents the 80% confidence limits on the change point (Figure 10). Faults from literature include Arava [*Janssen et al.*, 2004], Punchbowl [*Chester and Logan*, 1986], Muddy Mountain [*Brock and Engelder*, 1977], San Gabriel [*Chester et al.*, 2004], Kern Canyon (J. S. Chester, U.S. Geological Survey, Structure and petrology of the Kern Canyon Fault, California: A deeply exhumed strike-slip fault, final technical report, 2001), Pirgaki and Helike [*Micarelli et al.*, 2003], 90 Fathom [*Knott et al.*, 1996], Flower [*Sagy and Brodsky*, 2009], Bartlett [*Berg and Skar*, 2005], 100 m [*Beach et al.*, 1999], North and Glass [*Davatzes et al.*, 2003], and Lemont [*Fletcher and Savage*, 2007]. The Glass, North, Bartlett and *Beach et al.* [1999] faults include deformation bands.

Table 1. Fault Information for All Faults in Figures 5 and 9[a]

Fault	Fault Offset (m)	Fault Type	Depth of Faulting	Host Rock	Unit Thickness (m)	n	n Uncertainty	Width (m)	Number of Data Bins	Reference	Notes
Glass	38	n	2–4 km	Navajo sandstone	140–170	1.3	0.12	70	40	*Davatzes et al.* [2003]	counting fractures and deformation bands
Bartlett	170–300	n	not reported	Moab Member sandstone	23	0.98	0.07	246–268	35	*Berg and Skar* [2005]	counting fractures and deformation bands
North	28	n	2–4 km	Navajo sandstone	140–170	0.9	0.12	90	45	*Davatzes et al.* [2003]	counting fractures and deformation bands
Three Mile	1.2	n	1 km	Santa Cruz Mudstone	0.1–0.5	0.82	0.11	0.3–0.9	none	this study	counting tensile and shear fractures
Lemont	1.6	t	less than 2 km	carbonate	0.2	0.81	0.08	1.5	none	*Fletcher and Savage* [2007]	counting fractures, filled veins and stylolites
Ninety Fathom	140	n	not reported	sandstone		0.78	0.13	300	15	*Knott et al.* [1996]	counting deformation bands and fractures
Low Tide	0.35	n	1 km	Santa Cruz Mudstone	0.1–0.5	0.76	0.06	0.3–0.9	none	this study	counting tensile and shear fractures
Hackle	0.53	n	1 km	Santa Cruz Mudstone	0.1–0.5	0.67	0.11	0.32–1	none	this study	counting tensile and shear fractures
Helike	700–800	n	1–2 km	limestone		0.55	0.09	60–80	56	*Micarelli et al.* [2003]	depth estimate from *Labaume et al.* [2004]
Pirgaki	800–1,000	n	1–2 km	limestone		0.55	0.06	100	45	*Micarelli et al.* [2003]	depth estimate from *Labaume et al.* [2004]
Kern Canyon	15,000	ss	not reported	Wagy Flat Granodiorite		0.53	0.03	400	none	J. S. Chester (final technical report, 2001) USGS Annual Project Summary	counting fractures, veins and stylolites
Muddy Mountain	26,000	t	not reported	Aztec sandstone	~100	0.5	0.06	16	none	*Brock and Engelder* [1977]	counting fractures, offset estimate from *Fleck* [1970]
Beach et al. Fault	100	n	not reported	Nubian Sandstone		0.49	0.11	20	80	*Beach et al.* [1999]	counting deformation bands and small faults
Flower	100–200	n	surface	andesite	10	0.45	0.07	100	none	*Sagy and Brodsky* [2009]	counting fractures
Punchbowl	40,000	ss	2–4 km	sandstone, siltstone, conglomerate	0.01–5	0.4	0.03	140	none	*Chester and Logan* [1986] and *Wilson et al.* [2003]	
Arava	105,000	ss	>3 km	Wadi As Sir Limestone		0.37	0.12	300	none	*Janssen et al.* [2004]	
San Gabriel	21,000	ss	2–5km	gneiss		0.23	0.06	200	none	*Chester et al.* [2004]	counting fractures, faults and veins
Punchbowl	40,000	ss	2–4 km	schist				100–140		*Schulz and Evans* [2000]	
8 m fault	8	ss	1–2 km	sandstone	800–1400			6–19		*de Joussineau and Aydin* [2007]	fault core thickness not reported
14 m fault	14	ss	1–2 km	sandstone	800–1400			22–44		*de Joussineau and Aydin* [2007]	fault core thickness not reported
Lonewolf	80	ss	1–2 km	sandstone	800–1400			12–46		*de Joussineau and Aydin* [2007]	fault core thickness not reported
Wadi Araba	3	n	>1.5 km	Nubian sandstone				13		*Du Bernard et al.* [2002]	counting deformation bands
Carboneras	40,000	ss	4 km	mostly schist				1,000		*Faulkner et al.* [2003]	
Caleta Coloso	5,000	ss	6 km	granodiorite				500–600		*Mitchell and Faulkner* [2009]	
Multiple faults			not reported	Nubian Sandstone						*Beach et al.* [1999]	
Multiple faults				clastics						*Fossen and Hesthammer* [2000]	core data
Big Hole	variable along strike		1.5–3 km	Navajo sandstone	137–151			variable		*Shipton and Cowie* [2001]	counting deformation bands
Aigion	170	n	drilling reached 788 m	limestone				25		*Micarelli et al.* [2003]	fracture counting in drill core
San Andeas	320,000	ss	drilling reached 2.2 km	arenite, mudstone, siltstone, shale				250–300		*Bradbury et al.* [2007]	from cuttings and geophysical studies
Chelungpu	10–15 km	t	drilling reached 345 m	sandstones, shale, siltstone, mudstone				31–51		*Heermance et al.* [2003]	fracture counting in drill core
San Andreas	320,000	ss						150		*Li et al.* [2004]	seismic wave speed
Calico	10,000	ss						15,000		*Cochran et al.* [2009]	seismic wave speed

[a]The parameter n is the power law exponent from a least squares linear regression, as discussed in the text and plotted on Figures 5 and 15b. The n uncertainty is the mean absolute deviation from bootstrapping on 10,000 realizations. The fault types are n, normal; t, thrust; and ss, strike slip. The "number of data bins" notes whether fracture densities were binned by distance intervals, which can make the fracture falloff appear steeper. The "notes" describe the method of determining fracture density decay and/or fault thickness.

Table 2. Correlation Coefficients and Probability Values for All Faults in Figure 5[a]

Fault	Correlation Coefficient Power Law	Probability Value Power Law	Correlation Coefficient Exponential	Probability Value Exponential	Correlation Coefficient Logarithmic	Probability Value Logarithmic
Glass	0.72	4.84E-09	0.54	5.94E-06	0.74	2.39E-09
Bartlett	0.68	2.44E-27	0.63	4.19E-24	0.57	1.07E-20
Hackle	0.32	1.69E-05	0.37	2.75E-06	0.26	1.50E-04
North	0.59	1.08E-05	0.46	2.51E-04	0.61	6.48E-06
Helike	0.81	1.83E-06	0.84	7.10E-07	0.76	9.75E-06
Low Tide	0.43	3.00E-14	0.48	3.30E-16	0.32	3.20E-10
Three Mile	0.45	1.28E-07	0.44	2.52E-07	0.26	1.64E-04
Lemont	0.70	2.50E-09	0.76	6.95E-11	0.75	1.35E-10
Ninety Fathom	0.72	6.80E-05	0.70	9.65E-05	0.86	7.95E-07
Pirgaki	0.55	5.13E-09	0.37	8.80E-06	0.66	1.49E-11
Kern Canyon	0.80	1.87E-16	0.60	4.56E-10	0.68	2.55E-12
Muddy Mountain	0.70	4.99E-05	0.56	8.68E-04	0.74	2.18E-05
Flower	0.77	8.38E-05	0.61	1.64E-03	0.64	9.68E-04
Punchbowl	0.38	9.62E-12	0.27	2.27E-08	0.51	3.76E-17
Arava	0.33	6.34E-03	0.56	1.00E-04	0.45	8.22E-04
San Gabriel	0.36	2.35E-03	0.51	1.37E-04	0.31	5.70E-03
100 m	0.45	1.30E-03	0.44	1.30E-03	0.59	7.32E-05

[a]A linear correlation coefficient is used to determine the correlation between the field data and the least squares fit of the three different functions we tested. A larger coefficient (closer to one) represents a better correlation. The probability value represents the likelihood of exceeding the correlation coefficient in a random sample taken from an uncorrelated parent population, given the number of data points [*Bevington and Robinson*, 2003]. Small number represent small probabilities that the correlation came about randomly, i.e., a great deal of confidence in the fit.

separation. Whether separation or net slip is reported, the order of magnitude is all that is important on a log scale. Although reactivation could have occurred on any of the faults in the data set, thereby obscuring some of the offset that the fault has seen, this is equally likely on all faults in the data set and therefore may account for some noise in the data but cannot explain trends. Many host rock and fault types are included. The decay of fracture density away from a fault appears to be a nonlinear function of displacement. The density decay is fairly constant ($n \approx 0.8$) for smaller faults. On faults with displacement greater than ~150 m, the best fit damage decay exponent decreases with increasing displacement (this crossover scale is formally analyzed in section 5). The apparent falloff of damage with distance becomes more gradual as slip progresses beyond this threshold.

[12] Previous studies have found that the macrofracture and microfracture density decay is also well fit by a logarithmic or exponential function [*Chester et al.*, 2005; *Mitchell and Faulkner*, 2009]. We use the power law fit because the stresses produced from a line or point source, such as might be a realistic model of damaging fault slip, have power law decay [*Love*, 1927, chapter VIII]. Individual faults in this data set may be better fit by one of these functions (Table 2), and the change in decay behavior is captured when the whole data set is fit with any of these functional forms (although the trend is most apparent with power law or exponential fits; Figure 6). This implies that the evolution with displacement presented here is a general, physical phenomenon and not an artifact of our chosen functional form.

[13] Six of the studies within this compiled data set presented their fracture densities in binned format (gray points on Figure 5). In general, any smoothing has the effect of making the fracture density decay appear steeper (i.e., larger values of n) than the raw data. Figure 7 shows the effects of binning on the change in decay for the small faults in our study.

[14] Some of the studies within our data set measured multiple transects on the same fault. In order to show a representative view of the damage zone surrounding these faults, we include all of the transects when possible. This raises the question of how best to represent the average of these transects. For instance, the Punchbowl data in Figure 5 represent four individual transects [*Chester and Logan*, 1986; *Wilson et al.*, 2003], shown in Figure 8. For this

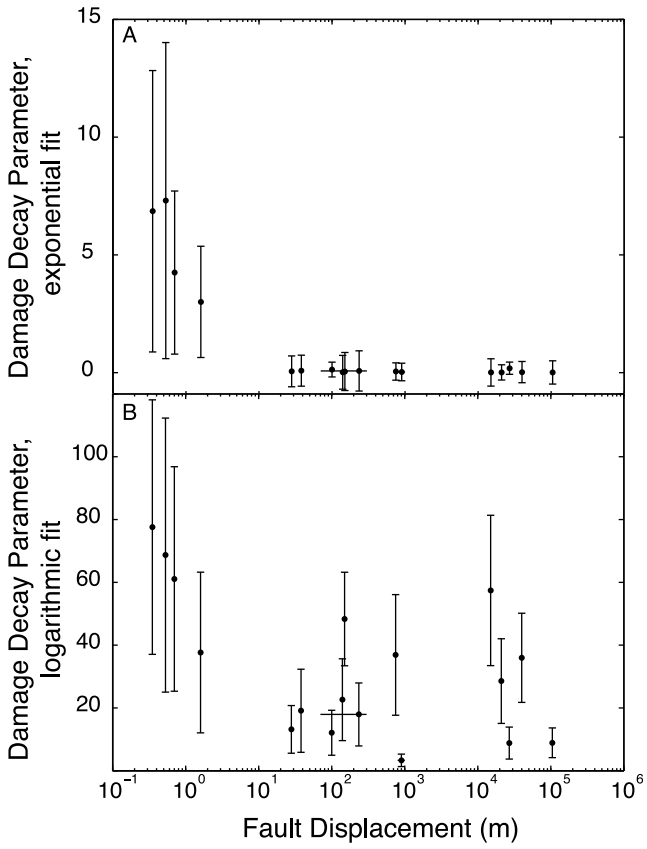

Figure 6. Change in decay parameters with displacement using (a) exponential and (b) logarithmic fits to the data.

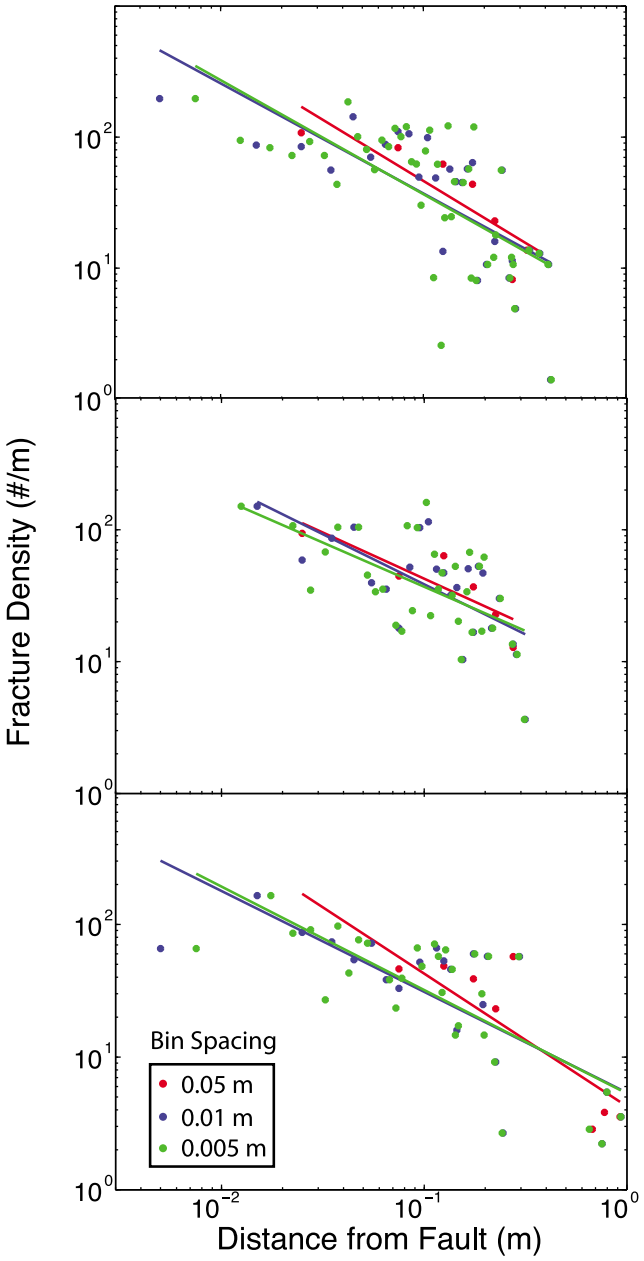

Figure 7. The fit to each data set is dependent on the number of bins used. Although the data presented in the paper for the Four Mile Beach faults are not smoothed in any way, certain faults within the larger data set are (see Table 1) and may have spuriously larger values of n.

study, we follow the original authors in fitting one function to a composite of the transects [*Chester et al.*, 2005] and fit these data with a power law function using a least squares method. Alternatively, each transect can be fit individually, and the average n can be used to determine falloff. We investigate both a weighted and nonweighted average.

[15] For the nonweighted average we take the mean from the 10,000 bootstrap realizations for each of the four individual transects and combine them to calculate mean and mean absolute deviation (Table 3). The mean absolute deviation is very large in this case, mostly because of transect DP15, which begins more than 10 m off the fault and is centered on a secondary fault. Therefore, this transect has negative value of n, i.e., increasing fracture density with distance. Because fitting this transect alone makes little sense as it was not meant to capture the falloff closer in to the fault, we also calculate the nonweighted mean and mean absolute deviation for the three transects which begin closer to the fault, which reduces the mean absolute deviation considerably. Table 3 shows that the nonweighted means and the composite fit are the same within uncertainty.

[16] For the weighted average, we penalize fits that have large variation by applying a weight that is equal to $1/\sigma$ where σ is the absolute deviation. The weighting considerably reduces the variation around the mean. The fits of DP15 and DP6 are so poor that they have little influence on the results. The weighted mean is slightly lower than the composite fit mean.

[17] We conclude that the mean value of the falloff exponent n calculated by any of these methods (composite method, unweighted mean of transects, or weighted mean of transects) results in similar values. However, the composite fit most accurately includes all of the data collected and therefore is used for Figure 5.

4. Total Fault Zone Thickness

[18] In addition to examining the fracture density decay, we also compiled measurements of total fault zone thickness (damage zone, as defined by the distance at which fracture density falls to the local background level, plus fault core thickness). We consider both the core and damage zone thickness here because cores may grow at the expense of damage zone thickness. When thickness for only one side of the fault is reported, we double the half thickness. *Scholz* [2002] suggested that damage zones grow as larger protrusions are encountered on a fractal fault with increasing displacement, therefore the ratio of fault thickness to displacement may be one. An opposing view is that damage zone thickness is more a function of local geometry (like fault linkages), and therefore highly variable along strike,

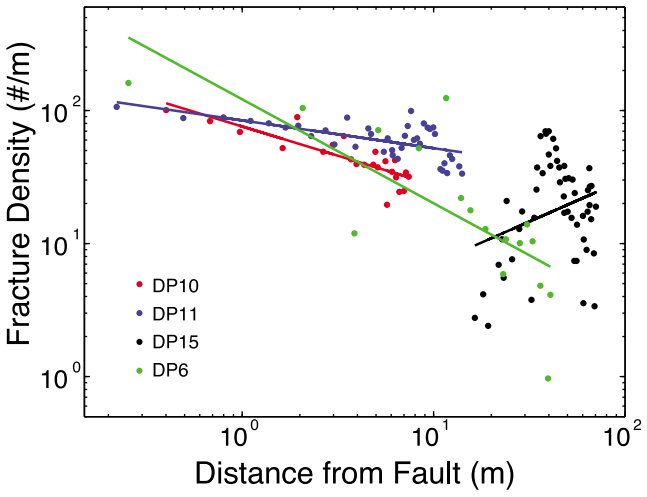

Figure 8. Four transects from the Punchbowl fault. Lines are power law fits to each individual transect. See text for discussion of the anomalous fit to transect DP15 which is centered on a secondary fault.

Table 3. Comparison of Methods to Combine Multiple Transects[a]

Power Law Exponent, n	All Transects Nonweighted	Three Transects Nonweighted	All Transects weighted	Composite Fit
Mean	0.27	0.54	0.26	0.4
Mean absolute deviation	0.43	0.28	0.02	0.04

[a]We did a least squares fit of a power law for the Punchbowl fault transects [*Chester and Logan*, 1986; *Wilson et al.*, 2003]. The mean exponent, n, was computed from 10,000 bootstrap realizations on the data set. The mean absolute deviation represents the residuals from the fit.

and independent of displacement [*Shipton et al.*, 2005]. Field studies and compilations show that damage zones grow linearly with displacement, but not at all locations along the fault [*Shipton and Cowie*, 2001] or that damage zone thickness is only subtly correlated with displacement, with most of the damage zone growing early in the fault slip history [*Childs et al.*, 2009]. We see steep fault zone growth with cumulative displacement until about 2400 m of displacement, and then fault zones grow much more gradually (Figure 9). Fracture density from drill cores [*Micarelli et al.*, 2003; *Heermance et al.*, 2003; *Bradbury et al.*, 2007] and estimates of fault zone thickness from studies of low-velocity zones around faults [*Li et al.*, 2004; *Cochran et al.*, 2009] agree with the field data, indicating that fracture measurements at the surface are not unduly influenced by exhumation.

5. Confirmation of Change in Slope Using Bayesian Information Criterion

[19] By performing a Bayesian information criterion (BIC) [*Main et al.*, 1999] analysis, we establish that the fracture falloff and width for the full suite of faults are indeed best fit by two slopes rather than a single function. In this method, the goodness of fit with two slopes is penalized for having extra fitting parameters. For two power laws, *Main et al.* [1999] formulated the BIC in log-log space for a combination of two linear regressions separated by the change point, x^*, to be optimized by the procedure. Therefore, the total of free parameters for two separate trends was 5 as opposed to 3 for a single regression with unknown variance. The BIC for the two slope fit is compared as a function of change point x* to the single regression. The fit with the maximum value of BIC is preferred. Thus, the method simultaneously ascertains how many free parameters are justified and the position of the slope break for a two-slope fit if it is the preferred model.

[20] In this application we utilize a constrained fit that reduces the number of free parameters and hence reduces the penalty associated with the BIC accordingly [see *Main et al.*, 1999, equation (4)]. For the density decay exponent n, we constrain the slope of the regression to the small fault data to be constant, thus reducing the number of free parameters by one. We use the unsmoothed data to establish the change

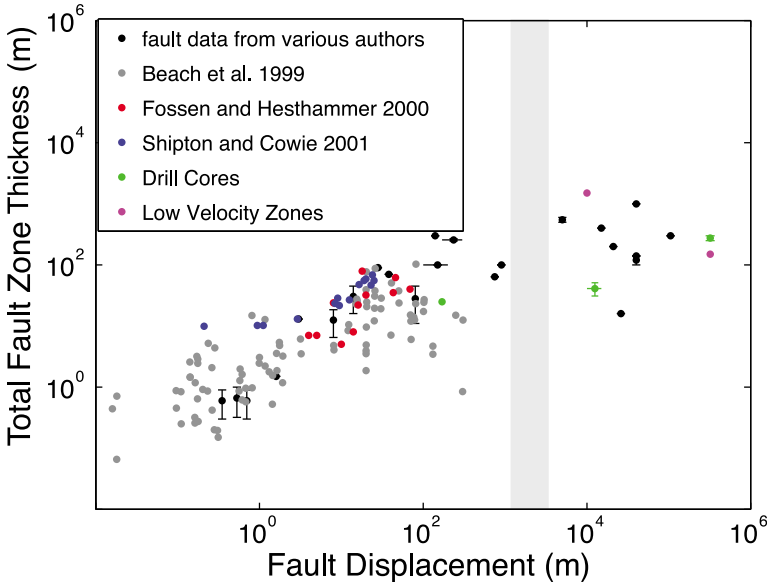

Figure 9. Total fault zone thickness as a function of fault displacement. The gray zone represents the 80% confidence limits on the change point (Figure 10). Field studies from literature include all of the faults referenced in Figure 5 as well as Punchbowl [*Schulz and Evans*, 2000], 8 m, 14 m, and Lonewolf [*de Joussineau and Aydin*, 2007], Caleta Coloso [*Mitchell and Faulkner*, 2009], Carboneras [*Faulkner et al.*, 2003], and Wadi Araba [*Du Bernard et al.*, 2002], and multiple faults from *Beach et al.* [1999] and multiple measurements along the Big Hole Fault [*Shipton and Cowie*, 2001]. Data from drill cores include Aigion [*Micarelli et al.*, 2003], Chelungpu [*Heermance et al.*, 2003], San Andreas [*Bradbury et al.*, 2007], and multiple faults from *Fossen and Hesthammer* [2000]. Low-velocity zones are plotted for San Andreas [*Li et al.*, 2004] and Calico faults [*Cochran et al.*, 2009]. The error bars represent a range of values reported. Additional information is available in Table 1.

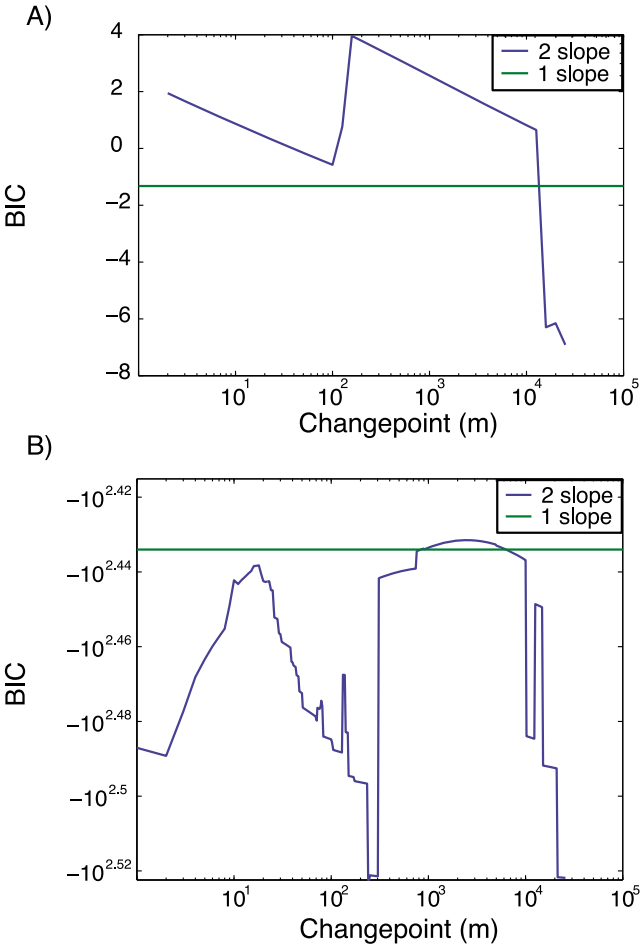

Figure 10. Bayesian information criteria (BIC) as a function of change point, x, for the double slope fit for (a) the fracture decay *n* and (b) the fault zone thickness.

point of *n* in Figure 5 in order to preserve homogeneity of data types. As noted above, binned data tends to steepen apparent fracture falloff. For fault thickness, we required that the regression slope for large faults be nonnegative, i.e., fault damage zones cannot become thinner with increasing displacement. The nonnegativity constraint does not affect the number of free parameters in the BIC calculation.

[21] Both the damage density decay and fault zone thickness are best fit by two slopes (Figure 10). For the fracture density falloff exponent *n*, the most likely change point is 151 m of displacement (150–1321 m with 80% confidence limits). The most likely change point for the fault zone thickness is ~2400 m of displacement (80% confidence interval 1514–3715 m).

6. Influence of Other Factors on Damage Zone Development

[22] Many factors have been shown to affect fracture spacing and fault development including depth of faulting, lithology, and layer thickness. We explore the effects of these parameters on damage density decay and fault zone thickness in our data set below. The style of faulting (strike-slip, thrust, normal) may affect damage zone development as well, but there is a dearth of thrust faults our data set (three) that make this analysis impossible at this time.

6.1. Depth of Faulting

[23] Damage zones are hypothesized to narrow with depth due to the increase in the strength of rock outside the fault zone [e.g., *Scholz*, 2002]. We plot the studies in our data set that reported a depth of faulting as a function of both decay exponent and total damage zone thickness (Figure 11). Depth of faulting shows a slight trend toward increasing fault zone thickness with depth; however, the two deepest faults also have large displacements (Caleta Coloso and Carboneras faults [*Faulkner et al.*, 2003; *Mitchell and Faulkner*, 2009]). The damage density decay exponent shows no relationship to depth of faulting.

6.2. Thickness of Fractured Layer

[24] Typically, the unit thickness of the layer being fractured is positively correlated with fracture spacing [e.g., *Pollard and Aydin*, 1988; *Bai and Pollard*, 2000]. In terms of fault damage zones, however, we find that the unit thickness is not the primary control of damage zone decay or fault zone thickness (Figure 12). Fault zone thickness may decrease with increasing unit thickness but there is no clear pattern for damage density decay in terms of unit thickness.

6.3. Lithology

[25] Different rock types have been shown to affect the development of fault zones [e.g., *Evans*, 1990]. Although we see little effect of lithology on total fault thickness, there

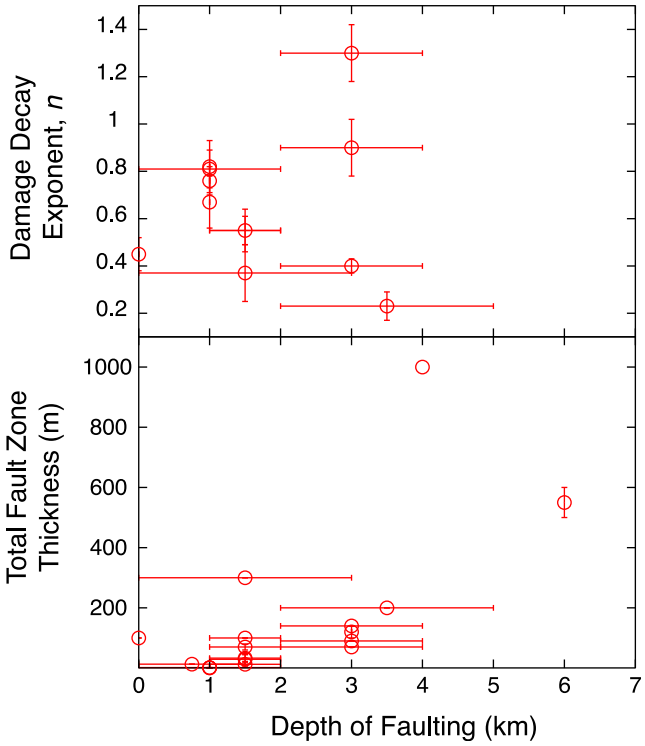

Figure 11. Depth of faulting controls on (top) fracture decay exponent and (bottom) fault zone thickness. Neither parameter shows a clear trend with depth of faulting, unlike displacement in Figures 5 and 9.

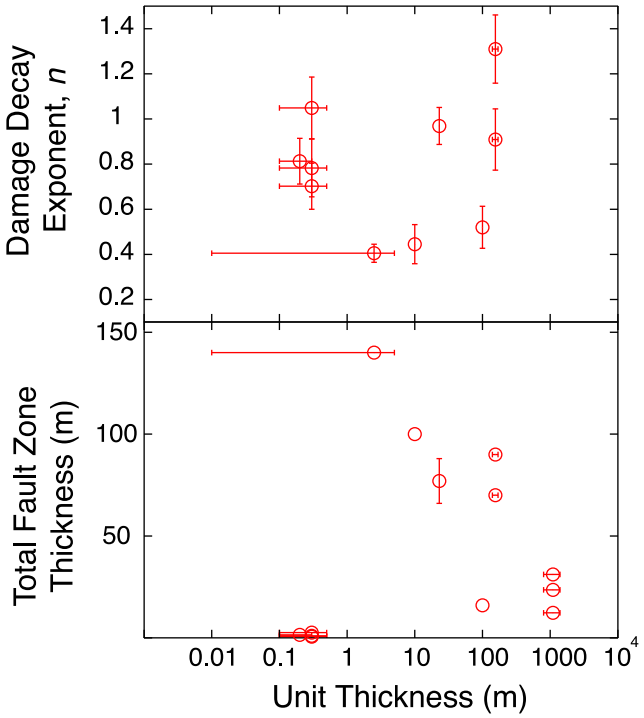

Figure 12. Unit thickness controls on (top) fracture decay exponent and (bottom) fault zone thickness. Neither parameter shows a clear trend with unit thickness, unlike displacement in Figures 5 and 9.

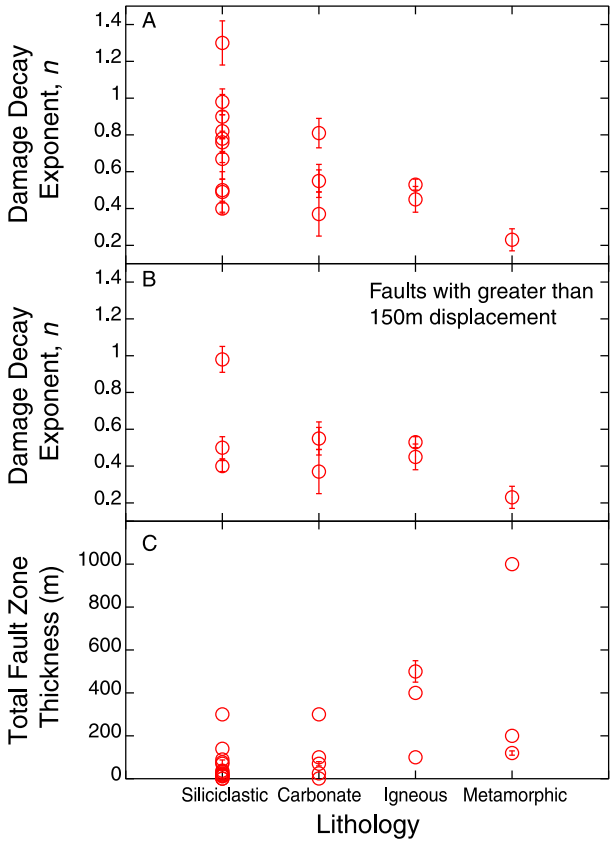

Figure 13. (a) Lithologic effects on decay exponent. The data indicate a lithological effect on density decay, with faults hosted in crystalline rocks showing a more gradual decay. (b) However, when only faults with greater than 150 m displacement are shown, which eliminates mostly small siliciclastic faults, the trend is erased. (c) Fault zone thickness shows minimal correlation with lithology.

is an effect of lithology on the decay exponent (Figure 13). However, most of the small faults in our study are in siliciclastic rocks, and displacement effects (which we argue are primary) are skewing the siliciclastic fault trend. Therefore, we remove all faults with less than 150m of displacement. There is no lithological effect on the decay exponent when the small faults are removed (Figure 13b).

6.4. Influence of Displacement on the Fault Constant *c*

[26] Just as the decay exponent *n* evolves with displacement, the constant *c* (equation (1)) changes with displacement as well. This parameter is related to the maximum density of fracturing in the host rock, and therefore will be lithology dependent. When we plot the entire data set shown in Figure 5, there is no clear relationship between *c* and displacement. However, when we sort the data set to include only the faults in siliciclastic sedimentary host rocks, we see that the value of *c* from the power law fit increases until around 150 m of displacement and then remains constant (Figure 14). This is expected since rock cannot be fractured indefinitely and remain a cohesive unit.

[27] The variations of *c* emphasize the value of the strategy of this study in focusing on n. The absolute fracture density is less consistent and more difficult to interpret than the decay of fracture with distance from the fault.

7. Interpretation: The Control of Secondary Strands on Damage Falloff

[28] We interpret the reduction in the best fit damage decay exponent with displacement in Figure 5 as a result of the distribution of slip onto secondary strands within the

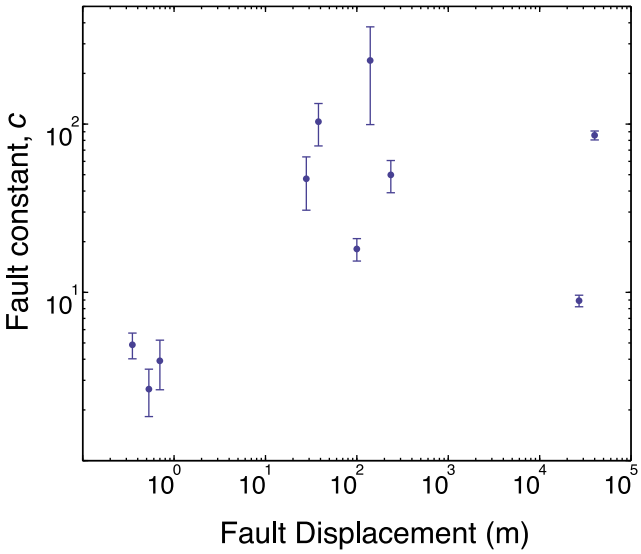

Figure 14. Fault constant, *c*, as a function of displacement for siliciclastic faults; *c* appears to increase with displacement until 150 m displacement has been achieved, at which point *c* ceases to increase.

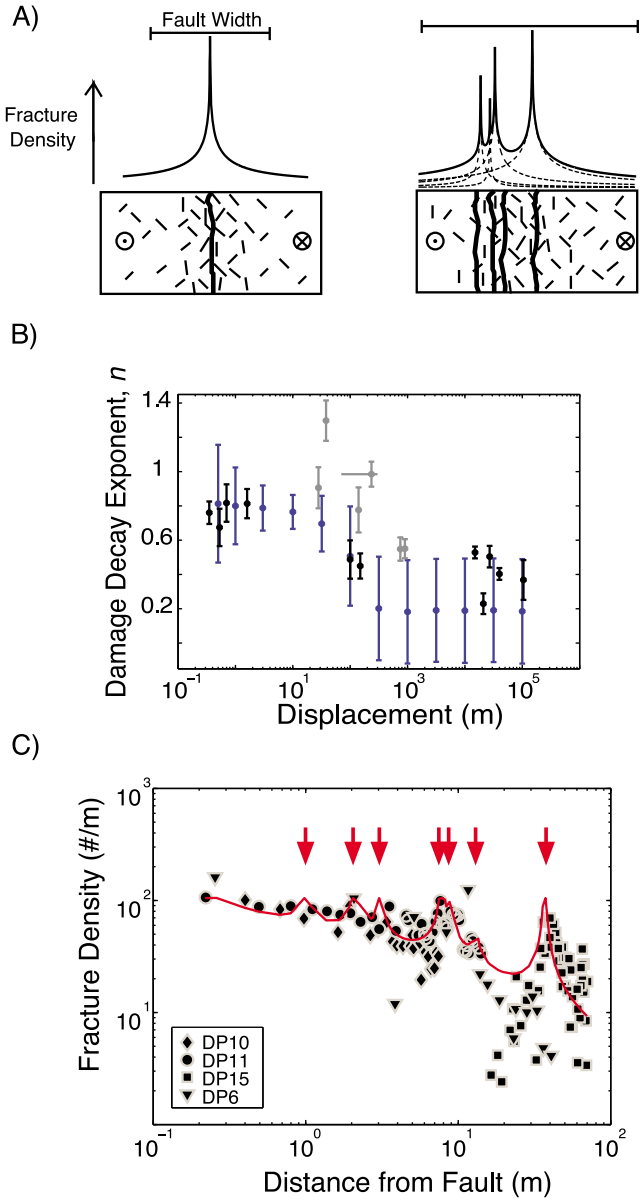

Figure 15. (a) Cartoon of fault zones with localized and distributed slip surfaces.(b) Stochastic model prediction of the damage decay exponent for p_{shear} = 0.05% (blue). Error bars are the mean absolute deviation from bootstrapping on 10,000 realizations. Data from Figure 5 are shown in black and gray, where gray represents faults with binned fracture densities. (c) Recreation of fracture distribution at the Punchbowl fault using a fracture decay of $r^{-0.8}$ for each reported secondary strand within the damage zone [*Chester and Logan*, 1986; *Wilson et al.*, 2003]. Arrows delineate the position of reported strands. A maximum fracture density of 106 fractures per meter (density closest to the main fault) was imposed, and the fault constant c was determined for each strand by the fit to the data.

damage zone. In our hypothesis, well-localized, isolated faults are expected to have a narrow decay of damage with distance from a strand. Faults with more secondary strands are expected to have a broader distribution of damage due to the superposition of multiple loci of fracturing (Figure 15a) [*Chester et al.*, 2004]. This superposition results in a change in the apparent decay from any one strand.

7.1. Stochastic Model of Fracture Density Decay

[29] To evaluate the plausibility of strand evolution influencing the observed damage decay with displacement, we utilize a simple stochastic model to combine the observations made from small and large faults. Stochastic simulations are a way of exploring a data set by imposing a small set of probabilistic rules governing the behavior in the distributions and then randomly sampling the proposed distributions to see how robustly the major observations are recreated. This method has been used to model fault networks [*Kagan*, 1982; *Harris et al.*, 2003] and aftershock sequences [*Ogata*, 1988]. The stochastic method allows us to explore the data, investigate hypotheses, and tease out various relationships. The appeal to this simplistic approach is that no specific physical mechanism (e.g., fault strand interaction, stress shadows) needs to be invoked, so that we can determine if the strand scenario is plausible without also determining the exact mechanics involved.

[30] We simulate the development of fault strands in a damage zone by distributing fractures throughout a set damage zone thickness, randomly allowing some of them to become secondary faults. The decay of damage away from a single fault is set as $r^{-0.8}$, as observed along the small faults in our study. In this way, we allow strands to form anywhere in the damage zone; however, they are more likely to form close to the main fault. The number of fractures in the system is generated proportional to the total displacement on the main fault and each new fracture has a very small probability of becoming a secondary fault with its own damage profile. This probability is the only free parameter in the model.

[31] We use a stochastic model to simulate the fracture distribution. We start by assigning a total number of fractures N to be simulated in the damage zone based on the total slip on the fault system S as

$$N = kS \tag{2}$$

where k is a constant for all faults. The total number of fractures that can be generated is capped at 1000. The

Table 4. Stochastic Model Parameters

Model Parameter	Value	Constraint
k	30 fractures per meter of slip	Average number of fractures in the damage zone of a fault divided by total displacement, based on faults at Four Mile Beach
x_{min}	3 mm	Smallest spacing between main fault and first fracture measured in the field studies in this paper
x_{max}	500 m	Half thickness of the largest fault thickness on Figure 5 (Carboneras Fault [*Faulkner et al.*, 2003])
p_{shear}	~0.05%	Free

Table 5. Comparison of the Different Functional Forms Fit to Punchbowl Fault Fracture Density Profile[a]

	Reduced Chi-Square	Probability Value
Composite	0.07	>0.99
Power Law	0.07	>0.99
Log	0.07	>0.99

[a]The chi-square values are reduced (chi-square/degrees of freedom). The probability value represents the probability of observing a value of reduced chi-square that is equal to or greater than the value we calculate from a random sample with a given number of samples and degrees of freedom. If the value is close to one, the assumed distribution describes the spread of data well [*Bevington and Robinson*, 2003].

thickness over which the fractures can be distributed is 500 m from the main strand, i.e., the half thickness of the thickest fault in the database [*Faulkner et al.*, 2003]; however, new damage zones on secondary strands can extend beyond that. We then distribute the N fractures in space using a stochastic algorithm where the requisite fracture distribution is obtained by inverting the uniform distribution [*Press et al.*, 2007, section 7.3]. The fracture distribution around an initial strand that is consistent with the small fault observations, i.e.,

$$p(x) = \frac{\int_{x_{\min}}^{x} \frac{1}{r^{0.8}} dr}{\int_{x_{\min}}^{x_{\max}} \frac{1}{r^{0.8}} dr} \tag{3}$$

where the normalization in the denominator is imposed so that the total probability of a fracture in the interval $x_{\min}$ to $x_{\max}$ is 1. The values of $x_{\min}$ and $x_{\max}$ as well as k are all determined from the field observations (Table 4). Equation (3) is implemented by randomly assigning a value of p for each of the N fractures and solving for x. As a result, the distance, x, of any particular fracture from the fault is described by

$$x = \left(x_{\min}^{0.2} + p\left(x_{\max}^{0.2} - x_{\min}^{0.2}\right)\right)^{0.5} \tag{4}$$

where p is a random number between 0 and 1. Each of the N fractures has a small probability, p_{shear}, of becoming a shear fracture. A fracture becomes the main fault strand when

$$1 - p_2 \leq p_{shear} \tag{5}$$

where p_2 is a random number between 0 and 1. If a new shear fracture is formed, then subsequent fractures of the N fractures in the population are distributed around that new origin using the same procedure as before (equation (4)).

[32] This stochastic model for developing fault strands is a function of the minimum distance between a shear surface and the closest fracture, the maximum distance from the fault at which fractures can form, the number of fractures generated per meter of slip and the probability that a fracture will become a fault strand (Table 4). Most of those variables are directly and independently constrained by the observational data. The value of $x_{\min}$ is the smallest distance measured between the fault and the first fracture at Four Mile Beach, $x_{\max}$ is the farthest distance from the fault that the fracture can form from the main fault, based on the half thickness of the largest damage zone in Figure 9 and the number of fractures per unit slip, k, is measured for two of the faults at Four Mile beach. The only free parameter is p_{shear}. We fit this parameter by requiring that the change in behavior occur around 150 m of fault displacement. We then generate simulations exploring values of p_{shear} that will match this fall off and find that that p_{shear} is tightly constrained by the data to fall at 0.05% (±0.04%).

[33] The model fits the data well (Figure 15b) and shows that the change in the best fit density decay exponent can arise from the generation of new strands. When the fault has experienced little displacement, there are few fractures in the damage zone. Since the expected number of strands is equal to the number of fractures multiplied by the probability of a fracture becoming a shear strand, for small slips the expected number of secondary strands is less than 1; that is, secondary strands are absent. As the number of fractures increases with slip, it becomes more likely that a strand will be present.

[34] The probability of a fracture becoming a shear fault in our model has to be very low (~0.05%) in order to fit the observed change in the best fit decay exponent at ~150 m. If we increase the probability, the observed change in the exponent occurs at smaller displacements. Faults form from the coalescence of fractures and the probability parameter may represent a critical crack density necessary for that coalescence [*Lockner et al.*, 1992], indicating that the damage zone needs to be heavily fractured before secondary strands start developing.

7.2. Strand Superposition on the Punchbowl Fault

[35] We illustrate the defocusing effect of strands on damage around a real fault with a well-documented example of a large-displacement fault. We create a composite curve by superposing damage peaks where secondary strands are reported along the Punchbowl Fault [*Chester and Logan*, 1986; *Wilson et al.*, 2003; *Chester et al.*, 2005]. We assume that each strand (including the main strand) has an $r^{-0.8}$ decay in fracture density, as per the small faults in our study, and sum the peaks to give the total damage zone decay (Figure 15c). The fracture density decrease is significantly matched by superimposing fault strands (Table 5). Although each individual transect has less than seven secondary faults, even one secondary fault located toward the edge of the damage zone can substantially alter the slope of the fracture decay. Figure 15c demonstrates that the superposition of peaks with steep falloffs is a viable model for the apparent shallowing of fracture density for large faults.

8. Discussion

[36] Previous work has evaluated the evolution of damage with displacement and proposed changes over a subset of the displacements or with different data types (i.e., microfractures) than considered here and found consistent results [*Beach et al.*, 1999; *Mitchell and Faulkner*, 2009]. This study is the first to cover displacements ranging over 5 orders of magnitude for both macroscopic fracture density decay and fault zone thickness at a wide range of localities and thus is the first work to observe the distinction in behavior for faults displaced more or less than ~150 m as a general feature. It is also the first work to interpret the change in behavior as due to the superposition

of a relatively simple damage decay as determined from isolated small faults.

[37] The $r^{-0.8}$ damage falloff from small faults noted in this study may be a result of the stress field around the fault during slip. The slope of the decay in stress with distance is in turn a function of the geometry of the source [*Love*, 1927, chapter VIII]. As noted by *Grady and Kipp* [1987], fracture density is proportional to stress raised to a power at a fixed stressing rate and therefore the observed damage falloff may be due to protrusions from the fault surfaces which act as mechanical strong points, i.e., irregularly shaped asperities [*Sagy and Brodsky*, 2009]. The change in slope in total fault thickness suggests that asperity size affects fault thickness [*Scholz*, 2002] for small faults but not for more mature faults. One possibility is that strand formation may allow for slip to be distributed throughout a zone, thereby making motion past large asperities possible without further damaging host rock. If there are fewer asperity collisions on more mature faults, then small earthquakes on immature faults should have more high-frequency energy than small earthquakes on mature faults. Indeed, recent work has shown that ground motions are larger for earthquakes on less mature faults [*Radiguet et al.*, 2009].

9. Conclusions

[38] We find that damage zones around all faults studied can be well fit by superposition of a simple form of damage decay. For faults with less than ~150 m of total displacement, damage decays as approximately the inverse of distance from the fault and fault zone thickness grows with displacement. Once a fault has slipped more than ~150 m, the apparent decay is much more gradual and fault zone thickness grows less with displacement. The weakening of the decay can be explained by the superposition of multiple fault strand damage peaks rather than a change in the individual fault damage decay. Secondary strands may nucleate when enough fractures are available to coalesce into shear planes. The break in scaling of damage zone thickness with displacement can be explained by the strand nucleation and does not require a change in physical processes between small and large faults.

[39] **Acknowledgments.** Field assistance from Nicholas van der Elst, Matt Johns, Steve Hartwell, Jacqui Gilchrist, Alicia Muirhead, and Julia Avila is much appreciated. We thank Michele Cooke, Ashley Griffith, James Kirkpatrick, Thorne Lay, Chris Marone, Casey Moore, Christie Rowe, Zoe Shipton, and Nicholas van der Elst for insightful comments on early drafts. The paper was improved due to comments from Jim Evans and an anonymous reviewer. This work was supported by NSF-OCE 0742242.

References

Anders, M. H., and D. V. Wiltschko (1994), Microfracturing, paleostress and the growth of faults, *J. Struct. Geol.*, *16*, 795–815, doi:10.1016/0191-8141(94)90146-5.

Bai, T., and D. D. Pollard (2000), Fracture spacing in layered rocks: A new explanation based on the stress transition, *J. Struct. Geol.*, *22*, 43–57, doi:10.1016/S0191-8141(99)00137-6.

Beach, A., A. I. Welbon, P. J. Brockbank, and J. E. McCallum (1999), Reservoir damage around faults: Outcrop examples from the Suez rift, *Petrol. Geosci.*, *5*(2), 109–116, doi:10.1144/petgeo.5.2.109.

Berg, S. S., and T. Skar (2005), Controls on damage zone asymmetry of a normal fault zone: Outcrop analyses of a segment of the Moab fault, SE Utah, *J. Struct. Geol.*, *27*, 1803–1822, doi:10.1016/j.jsg.2005.04.012.

Bevington, P. R., and P. R. Robinson (2003), *Data Reduction and Error Analysis for the Physical Sciences*, McGraw Hill, New York.

Bradbury, K. K., D. C. Barton, J. G. Solum, S. D. Draper, and J. P. Evans (2007), Mineralogical and textural analysis of drill cuttings from the San Andreas Fault Observatory at Depth (SAFOD) boreholes: Initial interpretations of fault zone composition and constraints on geologic models, *Geosphere*, *3*, 299–318, doi:10.1130/GES00076.1.

Brock, W. G., and J. T. Engelder (1977), Deformation associated with the movement of the Muddy Mountain overthrust in the Buffington window, southeastern Nevada, *Geol. Soc. Am. Bull.*, *88*, 1667–1677, doi:10.1130/0016-7606(1977)88<1667:DAWTMO>2.0.CO;2.

Chernyshev, S. N., and W. R. Dearman (1991), *Rock Fractures*, Butterworth-Heinemann, London.

Chester, F. M., and J. M. Logan (1986), Implications for mechanical properties of brittle faults from observations of the Punchbowl Fault Zone, California, *Pure Appl. Geophys.*, *124*, 79–106, doi:10.1007/BF00875720.

Chester, F. M., J. S. Chester, D. L. Kirschner, S. E. Schulz, and J. P. Evans (2004), Structure of large-displacement, strike-slip fault zones in the brittle continental crust, in *Rheology and Deformation in the Lithosphere at Continental Margins*, *Theoret. Exp. Earth Sci. Ser.*, vol. 1, edited by G. D. Karner et al., pp. 223–260, Columbia Univ. Press, New York.

Chester, J. S., F. M. Chester, and A. K. Kronenberg (2005), Fracture surface energy of the Punchbowl fault, San Andreas system, *Nature*, *437*(7055), 133–136, doi:10.1038/nature03942.

Childs, C., T. Manzocchi, J. J. Walsh, C. G. Bonson, A. N. Nicol, and M. P. J. Schopfer (2009), A geometric model of fault zone and fault rock thickness variations, *J. Struct. Geol.*, *31*, 117–127, doi:10.1016/j.jsg.2008.08.009.

Clark, J. C. (1981), Stratigraphy, paleontology, and geology of the central Santa Cruz Mountains, California Coast Ranges, *U.S. Geol. Surv. Prof. Pap.*, *1168*, 61.

Cochran, E. S., Y.-G. Li, P. M. Shearer, S. Barbot, Y. Fialko, and J. E. Vidale (2009), Seismic and geodetic evidence for extensive, long-lived fault damage zones, *Geology*, *37*(4), 315–318, doi:10.1130/G25306A.1.

Davatzes, N. C., A. Aydin, and P. Eichhubl (2003), Overprinting faulting mechanisms during the development of multiple fault sets in sandstone, Chimney Rock fault array, Utah, USA, *Tectonophysics*, *363*, 1–18, doi:10.1016/S0040-1951(02)00647-9.

de Joussineau, G., and A. Aydin (2007), The evolution of the damage zone with fault growth in sandstone and its multiscale characteristics, *J. Geophys. Res.*, *112*, B12401, doi:10.1029/2006JB004711.

Du Bernard, X., P. Labaume, C. Darcel, P. Davy, and O. Bour (2002), Cataclastic slip distribution in normal fault damage zones, Nubian sandstones, Suez rift, *J. Geophys. Res.*, *107*(B7), 2141, doi:10.1029/2001JB000493.

Evans, J. (1990), Thickness-displacement relationships for fault zones, *J. Struct. Geol.*, *12*(8), 1061–1065, doi:10.1016/0191-8141(90)90101-4.

Faulkner, D. R., A. C. Lewis, and E. Rutter (2003), On the internal structure and mechanics of large strike-slip fault zones: Field observations of the Carboneras fault in southeastern Spain, *Tectonophysics*, *367*(3–4), 235–251, doi:10.1016/S0040-1951(03)00134-3.

Fleck, R. J. (1970), Tectonic style, magnitude, and age of deformation in the Sevier orogenic belt in southern Nevada and eastern California, *Geol. Soc. Am. Bull.*, *81*(6), 1705–1720, doi:10.1130/0016-7606(1970)81[1705:TSMAAO]2.0.CO;2.

Fletcher, R. C., and H. M. Savage (2007), Coupling between brittle fracture and anticrack-vein pressure solution at asperities along a small-displacement thrust fault in limestone, *Eos Trans. AGU*, *88*(52), Fall Meet. Suppl., Abstract T33C-1497.

Fossen, H., and J. Hesthammer (2000), Possible absence of small faults in the Gullfaks Field, northern North Sea: Implications for downscaling of faults in some porous sandstones, *J. Struct. Geol.*, *22*(7), 851–863, doi:10.1016/S0191-8141(00)00013-4.

Grady, D. E., and M. E. Kipp (1987), Dynamic rock fragmentation, in *Fracture Mechanics of Rock*, edited by B. K. Atkinson, pp. 429–475, Academic, San Diego, Calif.

Harris, S. D., E. McAllister, R. J. Knipe, and N. E. Odling (2003), Predicting the three-dimensional population characteristics of fault zones: A study using stochastic models, *J. Struct. Geol.*, *25*(8), 1281–1299, doi:10.1016/S0191-8141(02)00158-X.

Heermance, R., Z. K. Shipton, and J. P. Evans (2003), Fault structure control on fault slip and ground motion during the 1999 rupture of the Chelungpu fault, Taiwan, *Bull. Seismol. Soc. Am.*, *93*, 1034–1050, doi:10.1785/0120010230.

Janssen, C., R. L. Romer, A. Hoffman-Rothe, D. Kesten, and H. Al-Zubi (2004), The Dead Sea Transform: Evidence for a strong fault?, *J. Geol.*, *112*, 561–575, doi:10.1086/422666.

Kagan, Y. Y. (1982), Stochastic model of earthquake fault geometry, *Geophys. J. Int.*, *71*, 659–691, doi:10.1111/j.1365-246X.1982.tb02791.x.

Knott, S. D., A. Beach, P. J. Brockbank, J. L. Brown, J. E. McCallum, and A. I. Welbon (1996), Spatial and mechanical controls on normal fault populations, *J. Struct. Geol.*, *18*(2–3), 359–372, doi:10.1016/S0191-8141(96)80056-3.

Labaume, P., E. Carrio-Schaffhauser, J.-F. Gamond, and F. Renard (2004), Deformation mechanisms and fluid-driven mass transfers in recent fault zones of the Corinth Rift (Greece), *C. R. Geosci.*, *336*(4–5), 375–383, doi:10.1016/j.crte.2003.11.010.

Li, Y. G., J. E. Vidale, and E. S. Cochran (2004), Low-velocity damaged structure of the San Andreas Fault at Parkfield from fault zone trapped waves, *Geophys. Res. Lett.*, *31*, L12S06, doi:10.1029/2003GL019044.

Lockner, D. A., J. D. Byerlee, V. Kuksenko, A. Ponomarev, and A. Sidorin (1992), Observations of quasi-static fault growth from acoustic emissions, in *Fault Mechanics and Transport Properties of Rocks*, edited by B. Evans and T.-F. Wong, pp. 3–31, Academic, San Diego, Calif., doi:10.1016/S0074-6142(08)62813-2.

Love, A. E. H. (1927), *A Treatise on the Mathematical Theory of Elasticity*, Dover, New York.

Main, I. G., T. Leonard, O. Papasouliotis, C. G. Hatton, and P. G. Meredith (1999), One slope or two? Detecting statistically significant breaks of slope in geophysical data, with application to fracture scaling relationships, *Geophys. Res. Lett.*, *26*(18), 2801–2804, doi:10.1029/1999GL005372.

Micarelli, L., I. Moretti, and J. M. Daniel (2003), Structural properties of rift-related normal faults: The case study of the Gulf of Corinth, Greece, *J. Geodyn.*, *36*(1–2), 275–303, doi:10.1016/S0264-3707(03)00051-6.

Mitchell, T. M., and D. R. Faulkner (2009), The nature and origin of off-fault damage surrounding strike-slip fault zones with a wide range of displacements: A field study from the Atacama fault system, northern Chile, *J. Struct. Geol.*, *31*, 802–816, doi:10.1016/j.jsg.2009.05.002.

Ogata, Y. (1988), Statistical models for earthquake occurrences and residual analysis for point processes, *J. Am. Stat. Assoc.*, *83*(401), 9–27, doi:10.2307/2288914.

Pollard, D. D., and A. Aydin (1988), Progress in understanding jointing over the past century, *Geol. Soc. Am. Bull.*, *100*, 1181–1204, doi:10.1130/0016-7606(1988)100<1181:PIUJOT>2.3.CO;2.

Press, W. H., S. A. Teukolsky, W. T. Vetterling, and B. P. Flannery (2007), *Numerical Recipes*, Cambridge Univ. Press, New York.

Radiguet, M., F. Cotton, I. Manighetti, M. Campillo, and J. Douglas (2009), Dependency of near-field ground motions on the structural maturity of the ruptured faults, *Bull. Seismol. Soc. Am.*, *99*(4), 2572–2581, doi:10.1785/0120080340.

Rice, J. R., C. Sammis, and R. Parsons (2005), Off-fault secondary failure induced by a dynamic slip pulse, *Bull. Seismol. Soc. Am.*, *95*(1), 109–134, doi:10.1785/0120030166.

Rispoli, R. (1981), Stress fields around strike-slip faults inferred from stylolites and tension gashes, *Tectonophysics*, *75*, T29–T36, doi:10.1016/0040-1951(81)90274-2.

Sagy, A., and E. E. Brodsky (2009), Geometric and rheological asperities in an exposed fault zone, *J. Geophys. Res.*, *114*, B02301, doi:10.1029/2008JB005701.

Scholz, C. H. (2002), *The Mechanics of Earthquakes and Faulting*, Cambridge Univ. Press, Cambridge, U. K.

Schulz, S. E., and J. P. Evans (1998), Spatial variability in microscopic deformation and composition of the Punchbowl fault, southern California: Implications for mechanisms, fluid-rock interaction, and fault morphology, *Tectonophysics*, *295*, 223–244, doi:10.1016/S0040-1951(98)00122-X.

Schulz, S. E., and J. P. Evans (2000), Mesoscopic structure of the Punchbowl Fault, southern California and the geologic and geophysical structure of active strike-slip faults, *J. Struct. Geol.*, *22*, 913–930, doi:10.1016/S0191-8141(00)00019-5.

Shipton, Z. K., and P. A. Cowie (2001), Damage zone and slip-surface evolution over μm to km scales in high-porosity Navajo sandstone, Utah, *J. Struct. Geol.*, *23*(12), 1825–1844, doi:10.1016/S0191-8141(01)00035-9.

Shipton, Z. K., J. P. Evans, and L. B. Thompson (2005), The geometry and thickness of deformation-band fault core and its influence on sealing characteristics of deformation-band fault zones, in *Faults, Fluid Flow, and Petroleum Traps*, edited by R. Sorkabi and Y. Tsuji, *AAPG Mem.*, 85, 181–195.

Shipton, Z. K., A. M. Soden, J. D. Kirkpatrick, A. M. Bright, and R. J. Lunn (2006), How thick is a fault? Fault-displacement-thickness scaling revisited, in *Earthquakes: Radiated Energy and the Physics of Faulting*, *Geophys. Monogr. Ser.*, vol. 170, edited by R. E. Abercrombie et al., 193–198 AGU, Washington, D. C.

Steele, R. G. D., and J. H. Torrie (1980), *Principles and Procedures of Statistics*, McGraw-Hill, New York.

Vermilye, J. M., and C. H. Scholz (1998), The process zone: A microstructural view of fault growth, *J. Geophys. Res.*, *103*(B6), 12,223–12,237, doi:10.1029/98JB00957.

Wilson, J. E., J. S. Chester, and F. M. Chester (2003), Microfracture analysis of fault growth and wear processes, Punchbowl Fault, San Andreas system, California, *J. Struct. Geol.*, *25*(11), 1855–1873, doi:10.1016/S0191-8141(03)00036-1.

E. E. Brodsky, Department of Earth and Planetary Sciences, University of California, 1156 High St., Santa Cruz, CA 95064, USA.

H. M. Savage, Lamont-Doherty Earth Observatory, Columbia University, 61 Route 9W, PO Box 1000, Palisades, NY 10964-8000, USA. (hsavage@ldeo.columbia.edu)